THE JOURNAL OF PHYSICAL CHEMISTRY C

Article

pubs.acs.org/JPCC

An XPS and UPS Study on the Electronic Structure of ThO_x ($x \leq 2$) Thin Films

Pelin Cakir,[†,‡] Rachel Eloirdi,*[,†] Frank Huber,[†] Rudy J. M. Konings,[†] and Thomas Gouder[†]

[†]European Commission, Joint Research Centre (JRC), Institute for Transuranium Elements (ITU), Postfach 2340, 76125 Karlsruhe, Germany

[‡]Faculty of Applied Sciences, Delft University of Technology, Mekelweg 15, 2629 JB Delft, The Netherlands

ABSTRACT: Model systems are needed for surface corrosion studies of spent nuclear oxide fuels. For this purpose ThO_2 films have been prepared in situ by adsorption of molecular and atomic oxygen on Th metal films and by sputter deposition of Th metal in an Ar/O_2 gas mixture. Surface compositions and electronic structure were compared to the bulk oxide and oxygen substoichiometry effects investigated. X-ray and ultraviolet photoemission spectroscopy (XPS and UPS, respectively) were used to measure to Th-4f, O-1s core levels and the valence band region. The Th-4f line was analyzed in terms of the final-state screening model. The evolution of the binding energies with oxygen concentration has been studied. On Th metal, adsorption of molecular oxygen ceased after the formation of a ThO_2 surface layer. In the presence of atomic oxygen, the oxidation proceeded into the underlying bulk. The formation of oxygen interstitials was shown by the broadening of the O-2p and O-1s lines and by the increase of the O-1s/Th-4f ratio. Once ThO_2 is formed, all photoemission peaks from Th and O undergo a rigid shift to low binding energy.

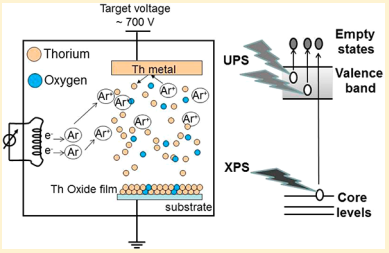

1. INTRODUCTION

Thorium is a potential future nuclear fuel.[1] There is a high natural abundance of the fertile ^{232}Th isotope. During operation, a smaller fraction of minor actinides is produced as compared to the U cycle,[1] so that it is quasi-inert, making it a candidate as an inert matrix to incinerate plutonium stockpiles. In this context, mixed oxides of Th with other actinides are worth being studied. Comparatively little information exists on thorium fuel, compared to uranium fuel forms,[2] because thorium based fuels have not been used commercially so far.

One important aspect for the application of nuclear fuels is the long-term stability of the waste. It depends on the resistance of the waste surface toward corrosion and dissolution in contact with groundwater.[3] To reach a better understanding and prediction of these processes,[4,5] surface science studies are being conducted, mainly on UO_2 fuel.[3,6,7] Only a few spectroscopy studies have been performed on $(U,Th)O_2$.[8] Because of the complexity of spent nuclear fuel, systematic studies of surface reaction mechanisms are difficult but can be realized by studying model systems, which focus on single reaction parameters. Fuel model systems can be prepared as thin films, starting with single actinide oxides, then processing to more complex systems, doping with fission products.[9] Such model films can be prepared by reactive sputtering from a series of elemental targets.[10] Thorium is the only actinide without 5f electrons. Its simplified chemistry, with only two oxidation states (0 and 4), makes it a very interesting reference material, indeed.

In this paper we discuss the preparation of ThO_2 films starting from the metal. Surface characterization, focusing on surface composition and electronic structure, is provided by photoemission spectroscopy following the core level Th-4f and O-1s by XPS and the valence band by UPS. The films are compared to bulk oxide compounds already reported in the literature[11,12] to ensure that there are no differences and that the films can really be used to model the bulk system. McLean et al.[11] performed an XPS and AES study of the surface oxidation of Th metal by O_2, CO, and CO_2 while Veal et al.[13] looked at both uranium and thorium as metal and dioxide forms. According to their results, the O-2p valence band spectra of UO_2 and ThO_2 are similar, but the 5f electron occupancy in UO_2 causes the difference between the two oxides, in particular electrical conductivity, color, and magnetism. Resonant photoemission spectra of the ThO_2 valence band have been compared to LMTO DOS calculations.[14] It was shown that there is a strong hybridization between O-2p and Th-6d orbitals. Riviéra[15] reported the surface potential of thorium films during the exposure of oxygen. His study shows that, once the surface of the film converted to ThO_2, oxygen does not diffuse into the metal further.

This paper is divided into two sections. First we investigate the reaction of the surface of thorium metal with oxygen, when exposed to molecular and atomic oxygen. Then, in a second part, we study the deposition of thin films of ThO_2 by argon sputtering in the presence of O_2. We follow the effect of the oxygen partial pressure on the surface oxidation and electronic structure of the sample. Possible oxygen off-stoichiometry (vacancies or interstitials) are investigated because they often

Received: July 7, 2014
Revised: September 26, 2014
Published: September 29, 2014

   dx.doi.org/10.1021/jp506750p | J. Phys. Chem. C 2014, 118, 24497−24503

are at the origin of enhanced reactivity. Substoichiometry oxides simulate oxygen vacancies. Their formation is tested by depositing Th in the presence of low oxygen partial pressure. Thorium cannot oxidize beyond Th^{4+} because it possesses only four valence electrons ([Rn] $6d^27s^2$), and supplementary surface oxygen cannot be incorporated into the lattice. We tested the accumulation of surface oxygen by chemisorption. While many surface characterization studies have been reported on UO_2 thin films,[16−19] it was important to report the first equivalent study on ThO_2 thin films, which will be used as a reference for a forthcoming study on $(U,Th)O_2$ films. The results obtained on ThO_x thin films are compared to those obtained previously on UO_x thin films.[16−18]

2. EXPERIMENTAL SECTION

The thin films of thorium metal and thorium oxide ThO_x ($x \leq 2$) were prepared in situ by direct current sputtering from a thorium metal target in Ar (6 N) and in a gas mixture of Ar (6 N) and O_2 (6 N), respectively. The oxygen concentration in the films was varied by adjusting the O_2 partial pressure (10^{-8}−8×10^{-7} mbar), while the Ar pressure was maintained at 5×10^{-7} mbar. The thorium target voltage was fixed at −700 V. The thin films were deposited at a rate of about 1 Å/s for 120 s at room temperature on a silicon wafers (111), which have been cleaned by Ar ion sputtering (4 keV) for 10 min, and subsequently annealed at 773 K for 5 min. The plasma in the diode source was maintained by injection of electrons (50−100 eV; triode setup) to work at low Ar pressure in the absence of stabilizing magnetic fields. Atomic oxygen was produced by an electron cyclotron resonance (ECR) Plasma Source Gen I from Tectra GmbH, Frankfurt/M. The atom flux is specified as $>10^{16}$ atoms cm^{-2} s, corresponding to an exposure of roughly 10 langmuirs/s (i.e., 10^{-5} mbar of O). After deposition, the thin films were transferred to the XPS-UPS analysis chamber via an interlock without exposing them to air.

Photoelectron spectroscopy data were recorded using a hemispherical analyzer from Omicron (EA 125 U5). The spectra were taken using Mg Kα (1253.6 eV) or Al Kα (1486.6 eV) radiation with an energy resolution of ∼1 eV. A few high-resolution XPS spectra were taken with a SPECS EA300 hemispherical analyzer using monochromated Al Kα radiation, yielding an energy resolution of 0.4 eV. UPS measurements were made using He II (40.81 eV) and He I (21.22 eV) radiation produced by a high-intensity windowless UV rare gas discharge source (SPECS UVS 300). The total resolution in UPS was 0.1−0.05 eV for the high-resolution scans. The background pressure in the analysis chamber was 2×10^{-10} mbar. The spectrometers was calibrated by using metallic Au-$4f_{7/2}$ at 83.9 eV BE and metallic Cu-$2p_{3/2}$ at 932.7 eV BE for XPS and on He I and He II Fermi edges for UPS. Photoemission spectra were taken at room temperature. The O/Th concentration ratio was determined by the ratio of the O-1s/Th-$4f_{7/2}$ surface areas, corrected by the atomic sensitivity factors.[20] The Th-4f and O-1s spectra were fitted by simple Gaussian functions. The inelastic background was subtracted by the Shirley algorithm.[21] The following equation has been used:[22]

$$n_O/n_{Th} = \frac{I_O/S_O}{I_{Th}/S_{Th}} \quad (1)$$

where n is the atomic concentration, I is the surface area of the main peak, O-1s and Th-$4f_{7/2}$, and S is the atomic sensitivity factor of 0.66 and 7.8 for O-1s and Th-$4f_{7/2}$, respectively.

An uncertainty of ±10% must be expected using tabulated values instead of internal references.[22]

The X-ray diffraction analyses were made on a conventional Phillips PW3830 powder diffractometer with a Cu anode ($K\alpha_1$ = 0.154 056 0 nm). Films of about 360 nm thicknesses were deposited (1 Å/s) at 100 °C on a Si (111) wafer and at room temperature on a Si (100) wafer.

3. RESULTS AND DISCUSSION

3.1. Oxygen Adsorption on Th Metal Film. Initial Th metal films were produced by sputtering Th onto a Si (111) substrate. The films were then exposed at room temperature to molecular oxygen until saturation and then to atomic oxygen. Figure 1 shows the corresponding Th-4f core level spectra.

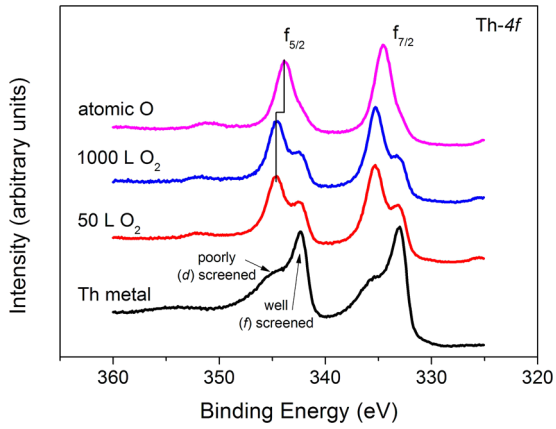

Figure 1. Th-4f spectra for Th metal film and after exposure to molecular and atomic oxygen.

They are split into the $4f_{5/2}$ and $4f_{7/2}$ components with a BE in the metal of 342.4 and 333.1 eV, respectively. Each peak has two components, associated with two different final states.[23,24] The well-screened peak (at low binding energy) corresponds to the final state where the 4f core hole of the ionized atom is screened by the population of a 5f-state, called f-screening. The poorly screened peak (at high binding energy) corresponds to the d-screened final state.[19] The well-screened peak occurs in the metal, while in ThO_2 oxide, the f-states become so high in energy that they no longer participate in the screening.[19,25]

After an exposure of 50 langmuirs of molecular oxygen (1 langmuir = $1 \text{ s} \times 10^{-6}$ Torr would provide one monolayer of gas particles, if the sticking probability is one) the poorly screened peak becomes dominant at the expense of the well-screened peak, the intensity of which decreases (Figure 1). The spectra are the same after exposure of 50 and 1000 langmuirs of O_2, showing the surface to be saturated. The presence of the well-screened peak indicates the contribution of the metal underneath the oxide layer. Indeed, the 4f spectrum of ThO_2 has only one component: the poorly (d) screened peak.[19] Quite remarkably, the 4f level of ThO_2 (in the presence of the metal) has the same binding energy as the poorly screened peak of the metal: as displayed in Figure 1, there is no shift to higher binding energy, which one would expect after oxidation.[26] The chemical shift links the binding energy to the oxidation state,[21] but this relation is not universal, and notably in the heavier actinides Am[27] and Cm,[12,28] the oxides have the same or even

dx.doi.org/10.1021/jp506750p | J. Phys. Chem. C 2014, 118, 24497−24503

lower core level binding energies than the metal. In all these cases, metal and oxide have the screening type (d-screening), and f-screening is minor either because the f-peak is too high in energy (Th) or because it is localized (Am, Cm).[12]

The spectrum after exposure to molecular oxygen (Figure 1, red and blue curve) still shows some metal left (at the position of the (f) screened peak). Oxidation is not complete in the region probed by XPS, which obtains a signal not only from the surface but also from deeper layers, which remain still metallic. The top surface, roughly estimated to 4.7 monolayers in our experimental conditions, is completely oxidized, and and on this surface, the dissociation of molecular oxygen is inhibited slowing down the diffusion through the oxide layer. Similar saturation after fast initial reaction has been observed for U metal.[11,29] After exposure to atomic oxygen (Figure 1, purple curve), the f-screened peak disappears completely, indicating all metal is oxidized to the depth probes by XPS. Atomic oxygen adsorbs on the oxide and subsequently diffuses through the oxide layer and reacts with the metal below. Thus, the rate-limiting step in the formation of the thin ThO_2 layers is the dissociation of molecular oxygen, not the bulk diffusion. After reaction with atomic oxygen the (d screened) 4f peak shifts to lower binding energy. We will discuss this below.

In the study by Rivière[15] on the surface potential of oxygen on thorium using the Kelvin method, it was reported that oxygen incorporation in the metallic lattice takes place before transformation of the saturated surface layers into ThO_2. Further oxygen cannot dissolve in ThO_2 as it does in UO_2 and it does not chemisorb on the ThO_2 surface at room temperature, so that, once the surface is saturated, oxygen diffusion into the bulk stops. The oxygen can reach the underlying metal by a mechanism of exchange with vacancies and not by interstitial diffusion. Part of this analysis is supported by the present study. Indeed O_2 adsorbs on the Th metal surface transforming it into ThO_2, covering the Th metal underneath. Then O_2 adsorption stops. Atomic oxygen continues to adsorb and diffuse into the bulk, oxidizing the metal into ThO_2.

The O-1s spectra after exposure to molecular and atomic oxygen are shown in Figure 2. Exposure to molecular oxygen leads to a sharp O-1s peak with a maximum at 531 eV BE and a weak shoulder at 532.5 eV. After exposure to atomic oxygen, the peak broadens considerably and higher BE component increases, which indicate chemisorption of oxygen at the surface

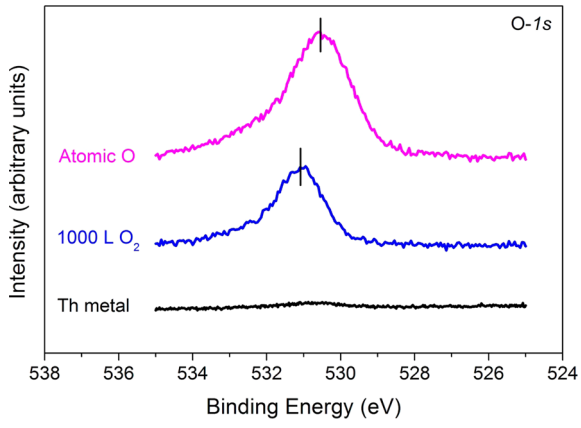

Figure 2. O-1s spectra of Th metal film and after exposure to molecular (bottom) and atomic oxygen (top).

because in this chemical form solid state relaxation is less strong.[30,31] This does not mean further oxidation of Th because similar adsorption was observed for MgO,[32−34] which cannot oxidize beyond Mg^{2+} and where the oxygen atoms bond to surface oxygen anions (in $O-O^-$ entities). The broadening of the peak, too, may be explained by oxygen build-up, resulting in nonequivalent surface oxygen atoms. The O-1s/Th-4f intensity ratio increases from 0.147 after molecular oxygen exposure to 0.201 after atomic oxygen. This increase indicates accumulation of oxygen, going from oxygen-deficient stoichiometry, formally ($ThO_{1.73}$), to oxygen-rich stoichiometry, formally ($ThO_{2.37}$), thorium oxide. $ThO_{2.37}$ is not a stable oxide, but this overstoichiometry is due to atomic oxygen chemisorbed on the surface. In addition, the film composition has been determined using general XPS sensitivity factors. Thus, an uncertainty of not better than 10% should be considered.[35]

After exposure to atomic oxygen, the O-1s shifts to lower BE. Th-4f undergoes the same shift (see Figure 1). So it is not a true chemical shift of one species in the crystal. A similar rigid shift has been observed in UO_2 upon surface oxidation, when the Fermi energy decreases due to charge carrier depletion[36,37] or to adsorbate induced band bending at the surface.[38] Since all photoemission lines in the (conductive) solid are referenced to the Fermi energy, a shift of the Fermi-level toward the core levels is seen as a coherent shift of all core-level lines to lower binding energy. ThO_2 is an insulator, but the thickness of the oxide layer (∼120 Å) seems small enough to allow electrons to tunnel through. Therefore, the Fermi level is still defined and the thin surface oxide film does not experience charging upon photoemission.[31]

The He II valence band spectra (Figure 3) allow studying the electrons levels participating in the oxidation process. The

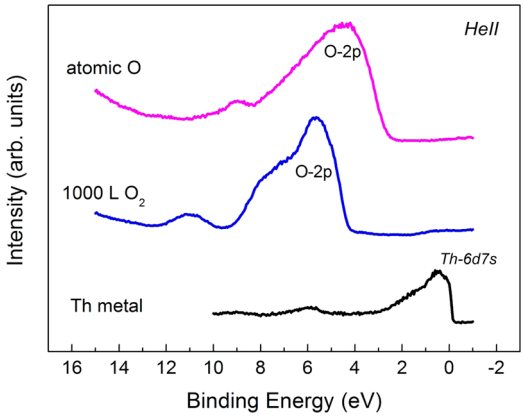

Figure 3. He II spectra for Th metal film and after exposure to molecular (bottom) and atomic oxygen (top).

metal film has a peak ranging from the Fermi level to 3 eV BE and corresponding to the Th-6d7s conduction band. After 1000 langmuirs of O_2, this peak totally disappears, and the O-2p valence band appears between 4 and 10 eV. As Th oxidizes to ThO_2, the 6d7s electrons are transferred into the O-2p band, leaving no states at the Fermi level. The high BE shoulder of the O-2p (8−9 eV) corresponds to the bonding part of the band, formed by Th-6d states hybridized with O-2p states. The maximum at low BE (5−6 eV) corresponds to the nonbonding part of the band.[39] In contrast to the Th-4f spectra, the oxidation observed in He II is complete and no trace of underlying metal is observed. The He II spectra are more

dx.doi.org/10.1021/jp506750p | J. Phys. Chem. C 2014, 118, 24497−24503

surface sensitive than the 4f (the inelastic mean free path is 1 instead of 5 layers[40]), and this confirms that the residual metal signal in the 4f data indeed came from deeper levels, and not from an incomplete reaction in the upper layers. The small signal at 11 eV comes from a small OH contamination, likely to be produced by water desorbed from the chamber walls. A shift of about 1.2 eV to lower binding energy is observed after exposure of the surface to atomic oxygen. As for the core level, it is attributed to the decrease of the Fermi energy concomitant with slight increase of the oxygen concentration. The O-2p is broadened, with supplementary intensity appearing at the high BE side, which is explained by supplementary oxygen, chemisorbed on the surface. It appears at high BE because of the lower relaxation energy available for chemisorbed species (less coordination).

Such oxygen is more visible in the surface sensitive UPS-He II spectra than in the bulk spectra, therefore the buildup of intensity at the high BE side is more pronounced than for the O-1s line.

3.2. Reactive DC Sputtering of ThO_x ($0 \leq x \leq 2$) Thin Films. Sputter deposition has been also used to prepare thin oxide films. In contrast to the previous method, there is no concentration gradient between the reacted surface and the bulk, but the films are homogeneous in composition. Thorium is sputtered from a thorium metal target in an Ar/O_2 gas mixture. Oxygen reacts with the metal atoms on the target, in the plasma and on the substrate. The oxygen composition of the film depends on the oxygen partial pressure in the chamber.

Figure 4 shows the Th-4f core level spectra of ThO_x at different O_2 partial pressures. In Figure 4 left, the spin−orbit

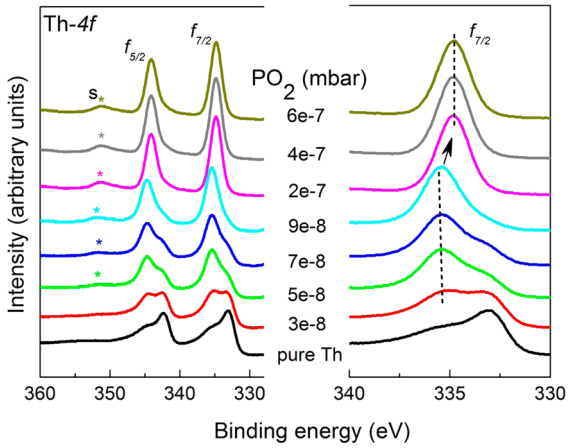

Figure 4. Left: Th-4f core level spectra of ThO_x ($0 \leq x \leq 2$) thin films versus O_2 partial pressure Right: zoom on corresponding Th-$4f_{7/2}$ core level spectra.

split $4f_{7/2}$ and $4f_{5/2}$ peaks can be followed, together with the appearance of a shakeup satellite peak(s) at 7.1 eV higher binding energy than the main peaks. Figure 4 right focuses on the Th-$4f_{7/2}$ component to emphasize the evolution of the peak shape and binding energy with oxygen partial pressure. As for O_2 adsorption, the f-screened component at low binding energy decreases with increasing oxygen pressure, as the Th metal consumes. The high BE component, consisting of the d-screened metal and oxide peak increases in intensity, replacing the f-screened peak completely at 9×10^{-8} mbar of O_2. Once all metal has reacted, the oxide line shifts to lower binding energy by about 0.7 eV (from 335.4 to 334.7 eV).

Figure 5 shows the spectrum of ThO_2 thin films obtained with a monochromated Al $K\alpha$ source. The main lines are

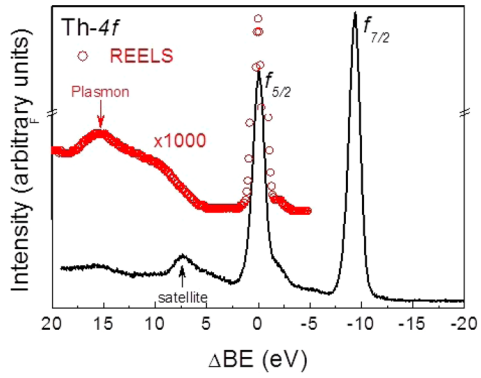

Figure 5. Th-4f core level spectra of ThO_2 thin film and superposition of corresponding plasmon signal measured by REELS. For better comparison, the spectra of Th-4f, normalized on the $4f_{5/2}$ component, and REELS are superimposed at same binding energy.

accompanied by two satellites at 7.5 and 15 eV, appearing at higher binding energy than the $f_{5/2}$ and $f_{7/2}$ peaks. The $f_{5/2}$ component is compared to a REELS (reflection electron energy loss spectroscopy) spectrum obtained with a primary electron beam of 1000 eV. The REELS spectrum indicates a band gap in the ThO_2 thin film of about 5.2 eV, which lies in the energy range reported for ThO_2 bulk (3.4−5.7 eV).[15] It also shows a plasmon loss feature at 15 eV and a weaker loss at 10 eV (associated with a surface plasmon: $\bar{\omega}_s = \bar{\omega}_b/\sqrt{2}$). The main Th-4f satellite at 7.4 eV higher BE than the main line is not a plasmon feature, but either a shake-up or a final-state satellite.[41]

The Fermi level shift of 0.7 eV observed at the formation of ThO_2 is smaller than the band gap measured by REELS. A similar observation has been reported for UO_2 thin film.[17] This has been related to the defects present in the layers produced by dc sputtering, pinning the Fermi level between the valence band and the conduction band. Thus, the Fermi level shift and the band gap cannot be correlated. The band gap for UO_2 was determined to be 2.1−2.7 eV,[13,42] which is smaller than the value found in this study for ThO_2 film and would be expected by the stronger insulator properties of ThO_2.

The O-1s spectra of the ThO_x ($0 \leq x \leq 2$) thin films are displayed in Figure 6. For pure Th metal, the oxygen peak can

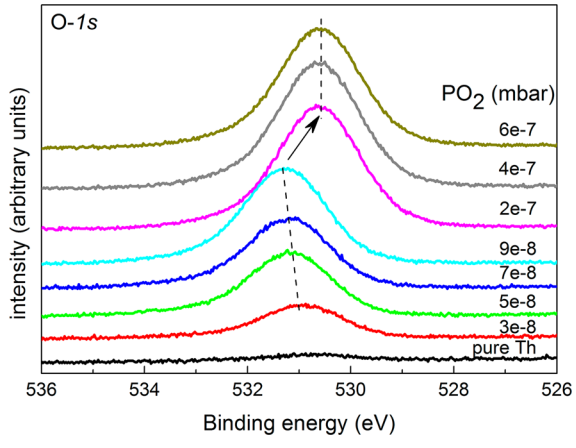

Figure 6. O-1s core level spectra as a function of O_2 partial pressure.

dx.doi.org/10.1021/jp506750p | J. Phys. Chem. C 2014, 118, 24497−24503

be hardly seen, which demonstrates the good sample purity. With increasing oxygen partial pressure the O-1s intensity increases. It first shifts to higher binding energy by 1.4 eV, and then at 9×10^{-8} mbar of O_2, it suddenly shifts back to low binding energy (by 0.7 eV), just as the Th-4f oxide peak (see above). The low BE shift occurs at the same oxygen pressure, i.e., once all metal contribution has disappeared. The shape of the peaks is highly symmetric and can be related to the good homogeneity of the films produced by dc sputtering.

Figure 7 shows He II valence band spectra of ThO_x ($x \leq 2$) thin films deposited at increasing O_2 partial pressure. Th metal

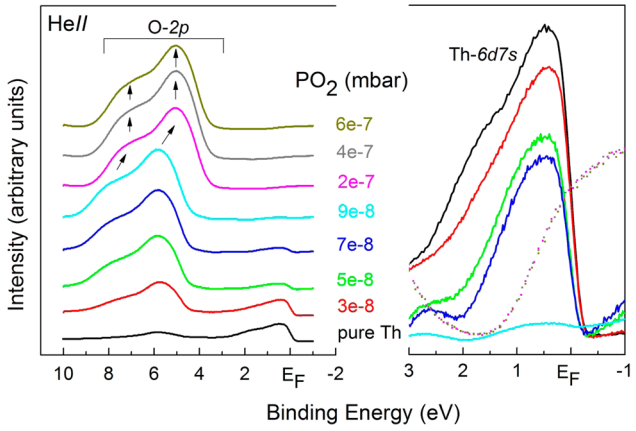

Figure 7. Left: He II spectra ThO_x ($0 \leq x \leq 2$) thin films versus O_2 partial pressure. Right: superposition of density of states of ThO_x ($0 \leq x \leq 2$) at Fermi level.

has a broad peak from 3 to 0 eV, attributed to the 6d7s conduction band. The small peak around 6 eV is due to the O-2p emission of a small oxygen contamination at the surface. With increasing O_2 pressure the conduction band peak decreases while the O-2p valence band peak grows between 5 and 9 eV. At 9×10^{-8} mbar of O_2, when all metal disappears (the emission at the Fermi level vanishes) the O-2p peak shifts to lower BE. This is the same shift as for the Th-4f and O-1s core level spectra, discussed earlier in this paper. The valence band spectra prove it to be associated with the disappearance of the metal.

Upon increasing oxygen concentration, the Th6d7s conduction band narrows (Figure 7, right). A similar narrowing has been observed for other valence and conduction band peaks upon dilution of metals in a host matrix, e.g., for U diluted in the weakly interacting Ag matrix,[43] of Au diluted in Ag.[44] Conversely, the O-2p line width of oxygen chemisorbed on metal surfaces increases with surface oxygen concentration. In all these case decrease of the spectral line width seems to reflect the narrowing of the bandwidth, due to spatial restriction or atomic isolation. In the present case a similar isolation of Th in the ThO_2 matrix would lead to a narrowing of the Th6d7s band. Oxide formation does not proceed via island growth (leaving large areas of metal unchanged) but proceeds homogeneously on the entire surface, disrupting the metal−metal bond.

Table 1 compares the binding energy of the thorium and oxygen core level obtained for ThO_2 thin film to the bulk values, obtained in this study and in the literature.[13,45] The values are in a good agreement emphasizing the interest and the capacity of using thin films as model for bulk samples.

Table 1. Binding Energy of Th-4f and O-1s, Peak Width, and Satellite Position Relatively to Main Peak Th-$4f_{7/2}$ Measured for ThO_2 Film and Bulk of This Study and Compared to Literature Data

	this study		literature
	thin film	bulk	bulk
Th-$4f_{7/2}$	334.8	334.5	334.6,[13] 334.9[45]
fwhm	1.85	2.32	1.8[13]
Th-$4f_{5/2}$	344.0	343.7	343.9[13]
satellite	7.3	7.6	7.3,[13] 6.9[45]
O-1s	530.6	530.4	

In Figure 8, we report the X-ray diffraction pattern of a ThO_2 film obtained by dc sputtering and deposited on Si (111) at 100

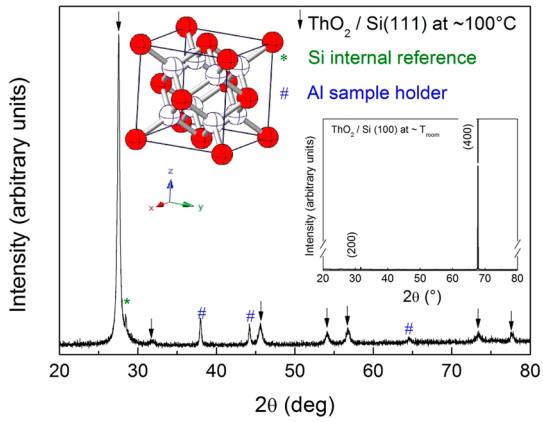

Figure 8. X-ray diffraction pattern of ThO_2 thin film deposited on Si(111) wafer at 100 °C and in inset on Si(100) at room temperature. Crystallographic structure of ThO_2.

°C. The (111) peak of Si is used as internal reference and despite the film thickness; we consider the sample height relatively to the Si surface negligible. The lattice parameter is calculated from the peak positions adjusted after the (111) Si peak was corrected to 2θ 28.44°[46] and obtained after extrapolation of $a = f(\sin^2 \theta)$. The pattern shows a polycrystalline structure corresponding to the cubic crystal structure expected for ThO_2 with a lattice parameter of a = 5.61 (1) Å, which is very close with the bulk lattice parameter, a = 5.598 (9) Å.[47] In the inset in Figure 8 the deposition of ThO_2 on Si (100) at room temperature is reported, and here we can see an epitaxial growth of the film along the direction (400). As reported for the deposition of UN films,[48] the microstructure of the sample is depending on the conditions of deposition, for instance the gas partial pressure, the temperature, and time of deposition. This has been the subject of complete experiments presented in the literature,[41,49] and this is out of the frame of the present study on the electronic structure, which is independent of the microstructure. However, this aspect is important due to its influence on the electrochemical behavior. Before to study the corrosion properties of ThO_2 and $(U,Th)O_2$ films, it is important to characterize their polycrystalline character to be representative as model of the fuel. The use of thin films as model for bulk fuel has the advantages that a large range of microstructure can be obtained going from single crystal to polycrystal, simulating different aspect of the nuclear fuel properties.

dx.doi.org/10.1021/jp506750p | J. Phys. Chem. C 2014, 118, 24497−24503

4. CONCLUSION

We have studied the formation and electronic structure of thin films of Th oxides using X-ray and ultraviolet photoemission spectroscopy. Thin films were prepared by exposing metal surfaces to oxygen or by depositing Th in the presence of oxygen (reactive sputtering).

When exposed to molecular oxygen, the thorium metal surface oxidizes quickly reaching saturation, while the subsurface stays metallic, with a characteristic Th-4f signal. The saturated surface reacts further with atomic oxygen, and eventually the bulk metal is transformed into oxide at room temperature. It is concluded that molecular oxygen does not dissociate on the oxide while atomic oxygen is still capable of adsorbing and diffusing into the bulk. Atomic oxygen adsorption broadens the O-2p valence band. All photoemission peaks underwent a rigid shift to low binding energy, which is consistent with the formation of O^{2-} surface atoms.

Thin films of ThO_x ($0 \leq x \leq 2$) were also produced by dc sputtering in Ar plasma with the presence of O_2. The film was continuously oxidized during formation, and there was no oxygen concentration gradient between surface and bulk. The Th-4f core level spectrum could be fitted by two peaks corresponding to f-screened and d-screened peak. While the f-screened peak is the main peak for the thorium metal, its BE shifts and its intensity decreases at the expense of the d-screened peak which is the main peak in ThO_2. The Th-4f and O-1s peaks both increase to higher binding energy until an O/Th ratio of about 2 and then drop suddenly to a lower and constant energy corresponding to the formation of ThO_2 which cannot further oxidized. The sudden drop of the binding energy observed for ThO_2 thin film is also attributed to the decrease of the Fermi energy. The advantage of working with thin films is that it avoids the charging effect which is observed on isolating bulk material.

Deposition of ThO_2 thin film on Si(111) wafer at 100 °C enable to produce a polycrystalline film with a preferential orientation along the ThO_2 (111) direction as demonstrated by X-ray diffraction. When the deposition is made at room temperature, an epitaxial growth takes place along the orientation of the support. It is apparent from these results that this method of using of actinide oxide thin films can be used for surface characterization and analysis without having pellets and bulk materials.

AUTHOR INFORMATION

Corresponding Author

*E-mail Rachel.Eloirdi@ec.europa.eu; Tel +49 (0) 7247 951803 (R.E.).

Notes

The authors declare no competing financial interest.

ACKNOWLEDGMENTS

We thank G. Pagliosa for his technical support in the X-ray diffraction analyses and Prof. R. Caciuffo and J. Somers for fruitful discussions. P. Cakir acknowledges the European Commission for support in the frame of the Training and Mobility of Researchers programme.

REFERENCES

(1) IAEA, Role of Thorium to Supplement Fuel Cycles of Future Nuclear Energy Systems. IAEA Nuclear Energy Series No. NF-T-2.4, 2012.

(2) Crawford, D. C.; Porter, D. L.; Hayes, S. L. Fuels for Sodium-Cooled Fast Reactors: US Perspective. *J. Nucl. Mater.* **2007**, *371*, 202–231.

(3) Hedhili, M. N.; Yakshinskiy, B. V.; Madey, T. E. Interaction of Water Vapor with UO_2 (001). *Surf. Sci.* **2000**, *445*, 512–525.

(4) Geckeis, H.; Rabung, T. Actinide Geochemistry: From the Molecular Level to the Real System. *J. Contam. Hydrol.* **2008**, *102*, 187–95.

(5) Kim, J. Significance of Actinide Chemistry for the Long-Term Safety of Waste Disposal. *Nucl. Eng. Technol.* **2006**, *38*, 459–482.

(6) Allen, G. C.; Tucker, P. M.; Tyler, J. W. Oxidation of Uranium Dioxide at 298 K Studied by Using X-ray Photoelectron Spectroscopy. *J. Phys. Chem.* **1982**, *86*, 224–228.

(7) Winer, K.; Colmenares, C. A.; Smith, R. L.; Wooten, F. Interaction of Water Vapor With Clean and Oxygen-Covered Uranium Surfaces. *Semin. Thorac. Cardiovasc. Surg. Pediatr. Card. Surg. Annu.* **1987**, *183*, 67–99.

(8) Sunder, S.; Miller, N. H. XPS and XRD Studies of $(Th,U)O_2$ Fuel Corrosion in Water. *J. Nucl. Mater.* **2000**, *279*, 118–126.

(9) Stumpf, S.; Seibert, A.; Gouder, T.; Huber, F.; Wiss, T.; Römer, J.; Denecke, M. A. Development of Fuel-Model Interfaces: Characterization of Pd Containing UO_2 Thin Films. *J. Nucl. Mater.* **2010**, *397*, 19–26.

(10) Gouder, T. Thin Layers in Actinide Research. *J. Alloys Compd.* **1998**, *271–273*, 841–845.

(11) Mclean, W.; Colmenares, C. A.; Smith, R. L. Electron-Spectroscopy Studies of Clean Thorium and Uranium Surfaces. Chemisorption and Initial Stages of Reaction with O_2, CO, and CO_2. *Phys. Rev. B* **1982**, *25*, 8–24.

(12) Veal, B. W.; Lam, D. J.; Diamond, H.; Hoekstra, H. R. X-ray Photoelectron-Spectroscopy Study of Oxides of the Transuranium Elements Np, Pu, Am, Cm, Bk, and Cf. *Phys. Rev. B* **1977**, *15*, 2929–2942.

(13) Veal, B. W.; Lam, D. J. X-ray Photoelectron Studies of Thorium, Uranium, and Their Dioxides. *Phys. Rev. B* **1974**, *10*, 4902–4908.

(14) Ellis, W. P.; Boring, A. M.; Allen, J. W.; Cox, L. E.; Cowan, R. D.; Pate, B. B.; Arko, A. J.; Lindau, L. Valance-Band Photoemission Intensities in Thorium Dioxide. *Solid State Commun.* **1989**, *72*, 725–729.

(15) Riviere, J. C. The Surface Potential of Oxygen on Thorium. *Br. J. Appl. Phys.* **1965**, *16*, 1507–1511.

(16) Bao, Z.; Springell, R.; Walker, H. C.; Leiste, H.; Kuebel, K.; Prang, R.; Nisbet, G.; Langridge, S.; Ward, R. C. C.; Gouder, T.; et al. Antiferromagnetism in UO_2 Thin Epitaxial Films. *Phys. Rev. B* **2013**, *88*, 134426(1)–134426(10).

(17) Miserque, F.; Gouder, T.; Wegen, D. H.; Bottomley, P. D. W. Use of UO_2 Films for Electrochemical Studies. *J. Nucl. Mater.* **2001**, *298*, 280–290.

(18) Van den Berghe, S.; Miserque, F.; Gouder, T.; Gaudreau, B.; Verwerft, M. X-ray Photoelectron Spectroscopy on Uranium Oxides: A Comparison Between Bulk and Thin Layers. *J. Nucl. Mater.* **2001**, *294*, 168–174.

(19) Stumpf, S.; Seibert, A.; Gouder, T.; Huber, F.; Wiss, T.; Römer, J. Development of Fuel-Model Interfaces: Investigations by XPS, TEM, SEM and AFM. *J. Nucl. Mater.* **2009**, *385*, 208–211.

(20) Wagner, C. D.; Davis, L. E.; Zeller, M. V.; Taylor, J. A.; Raymond, R. H.; Gale, L. H. Empirical Atomic Sensitivity Factors for Quantitative Analysis by Electron Spectroscopy for Chemical Analysis. *Surf. Interface Anal.* **1981**, *3*, 211–225.

(21) Shirley, D. A. High-Resolution X-Ray Photoemission Spectrum of the Valence Bands of Gold. *Phys. Rev. B* **1972**, *5*, 4709–4714.

(22) Seah, M. P. The Quantitative Analysis gf Surfaces by XPS. *Surf. Interface Anal.* **1980**, *2*, 222–239.

(23) Gunnarsson, O.; Sarma, D. D.; Hillebrecht, F. U.; Schönhammer, K. Electronic Structure of the Light Actinide Oxides From Electron Spectroscopy (Invited). *J. Appl. Phys.* **1988**, *63*, 3676–3679.

(24) Moore, K. T.; Van der Laan, G. Nature of the 5f States in Actinide Metals. *Rev. Mod. Phys.* **2009**, *81*, 235–298.

(25) Hufner, S.; Wertheim, G. K. Systematic of Core Line Asymmetries in XPS Spectra of Ni. *Phys. Lett.* **1975**, *51A*, 301−303.
(26) Chusuei, C. C.; Goodman, D. W. In *X-ray Photoelectron Spectroscopy. Encyclopedia of Physical Science and Technology*; Meyers, R. A., Ed.; Academic Press: New York, 2002; Vol. *17*, pp 921−938.
(27) Gouder, T.; Oppeneer, P. M.; Huber, F.; Wastin, F.; Rebizant, J. Photoemission Study of the Electronic Structure of Am, AmN, AmSb, and Am_2O_3 Films. *Phys. Rev. B* **2005**, *72*, 115122(1)−115122(7).
(28) Gouder, T.; Van der Laan, G.; Shick, A. B.; Haire, R. G.; Caciuffo, R. Electronic Structure of Elemental Curium Studied by Photoemission. *Phys. Rev. B* **2011**, *83*, 125111(1)−125111(6).
(29) Gouder, T.; Colmenares, C.; Naegele, J. R.; Verbist, J. Study of the Surface Oxidation of Uranium by UV Photoemission Spectroscopy. *Surf. Sci.* **1989**, *235*, 280−286.
(30) Bloch, J.; Atzmony, U.; Dariel, M. P.; Mintz, M. H.; Shamir, N. Surface Spectroscopy Studies of the Oxidation Behavior of Uranium. *J. Nucl. Mater.* **1982**, *105*, 196−200.
(31) Over, H.; Seitsonen, A. P. Surface Chemistry: Oxidation of Metal Surfaces. *Science* **2002**, *297*, 2003−2005.
(32) Ghijsen, J.; Namba, H.; Thiry, P. A.; Pireaux, J. J.; Caudano, P. Adsorption of Oxygen on the Magnesium (0001) Surface Studied by XPS. *Appl. Surf. Sci.* **1981**, *8*, 397−411.
(33) Corneille, J. S.; He, J.; Goodman, D. W. XPS Characterization of Ultra-Thin MgO Films on a Mo(100) Surface. *Surf. Sci.* **1994**, *306*, 269−278.
(34) Fanjoux, G.; FornanderBillault, H.; Lescop, B.; Le Nadan, A. Evolution of the Magnesium Surface during Oxidation Studied by Metastable Impact Electron Spectroscopy. *J. Electron Spectrosc. Relat. Phenom.* **2001**, *119*, 57−67.
(35) Seah, M. P. Recent Advances To Establish XPS as an Accurate Metrology Tool. *J. Surf. Anal.* **2006**, *13*, 136−141.
(36) Cros, A. Charging Effects in X-ray Photoelectron. *J. Electron Spectrosc. Relat. Phenom.* **1992**, *59*, 1−14.
(37) Cazaux, J. Mechanisms of Charging in Electron Spectroscopy. *J. Electron Spectrosc. Relat. Phenom.* **1999**, *105*, 155−185.
(38) Zhand, Z.; Yates, T. Band Bending in Semiconductors: Chemical and Physical Consequences at Surfaces and Interfaces. *Chem. Rev.* **2012**, *112*, 5520−5551.
(39) Teterin, A.; Ryzhkov, M.; Teterin, Y.; Vukcevic, L.; Terekhov, V.; Maslakov, K.; Ivanov, K. Valence Electronic State Density in Thorium Dioxide. *Nucl. Technol. Radiat. Prot.* **2008**, *23*, 34−42.
(40) Bubert, H.; Riviere, J. C. Photoelectron Spectroscopy. In *Surface and Thin Film Analysis*; Bubert, H., Jenett, H., Eds.; VCH: Weinheim, 2002; pp 6−32.
(41) Kotani, A.; Yamazaki, T. Systematic Analysis of Core Photoemission Spectra for Actinide Di-Oxides and Rare-Earth Sesqui-Oxides. *Prog. Theor. Phys. Suppl.* **1992**, *108*, 117−131.
(42) Winter, P. W. The Electronic Transport Properties of UO_2. *J. Nucl. Mater.* **1989**, *161*, 38−43.
(43) Eloirdi, R.; Gouder, T.; Korzhavyi, P. A.; Wastin, F.; Rebizant, J. Dilution Effect on the U-5f States: U in an Ag Matrix. *J. Alloys Compd.* **2005**, *386*, 70−74.
(44) Bzowski, A.; Kuhn, A.; Sham, T. K.; Rodriguez, J. A.; Hrbek, J. Electronic Structure of Au-Ag Bimetallics: Surface Alloying on Ru(001). *Phys. Rev. B* **1999**, *59*, 13379−13393.
(45) Allen, G. C.; Hubert, S.; Simoni, E. Optical Absorption and X-ray Photoelectron Spectroscopic Studies of Thorium Tetrabromide. *J. Chem. Soc., Faraday Trans.* **1995**, *91*, 2767−1769.
(46) Bond, W. L.; Kaiser, W. Interstitial versus Substitutional Oxygen in Silicon. *J. Phys. Chem. Solids* **1960**, *16*, 44−45.
(47) Hubert, S.; Purans, J.; Heisbourg, G.; Moisy, P.; Dacheux, N. Local Structure of Actinide Dioxide Solid Solutions $Th_{1-x}U_xO_2$ and $Th_{1-x}Pu_xO_2$. *Inorg. Chem.* **2006**, *45*, 3887−3894.
(48) Rafaja, D.; Havela, L.; Kužel, R.; Wastin, F.; Colineau, E.; Gouder, T. Real Structure and Magnetic Properties of UN Thin Films. *J. Alloys Compd.* **2005**, *386*, 87−95.
(49) Havela, L.; Miliyanchuk, K.; Rafaja, D.; Gouder, T.; Wastin, F. Structure and Magnetism of Thin UX Layers. *J. Alloys Compd.* **2006**, *408−412*, 1320−1323.